J. Fluid Mech. (2021), *vol.* 927, R5, doi:10.1017/jfm.2021.808

JFM RAPIDS

On the Alber equation for shoaling water waves

Mateusz Kluczek[1], **David Andrade**[1,†] **and Michael Stiassnie**[1]

[1]Department of Civil and Environmental Engineering, Technion, 3200003 Haifa, Israel

(Received 28 July 2021; revised 24 August 2021; accepted 10 September 2021)

The problem of unidirectional shoaling of a water-wave field with a narrow energy spectrum is treated by using a new Alber equation. The stability of the linear stationary solution to small non-stationary disturbances is analysed; and numerical solutions for its subsequent long-distance evolution are presented. The results quantify the physics which causes the gradual decay in the probability of freak-wave occurrence, when moving from deep to shallow coastal waters.

Key words: surface gravity waves, topographic effects

1. Introduction

Beginning with a Schrödinger equation in infinite or constant depth as their starting point, Longuet-Higgins (1976) and Alber (1978) obtained two rather different stochastic evolution equations.

Longuet-Higgins assumed that the wave field is a homogeneous and nearly Gaussian random process. His result is actually the narrow-band limit of the Hasselmann kinetic equation.

Alber, on the other hand, enabled the random process to be inhomogeneous but required Gaussianity. He used his equation to study the instability of a homogeneous wave field to inhomogeneous disturbances. Alber's findings are actually the stochastic counterpart of the well-known deterministic Benjamin–Feir instability, which can be described with the cubic Schrödinger equation.

From the cubic Schrödinger equation, it is known that the Benjamin–Feir instability leads not to a permanent end state, but to an unsteady series of modulation and demodulation cycles, called the Fermi–Pasta–Ulam recurrence phenomenon. Stiassnie, Regev & Agnon (2008) solved the Alber equation in infinite depth numerically and showed that a stochastic parallel to the Fermi–Pasta–Ulam recurrence exists. This stochastic recurrence enabled them to study the probability of waves that are higher than

† Email address for correspondence: deandradep@gmail.com

© The Author(s), 2021. Published by Cambridge University Press. This is an Open Access article, distributed under the terms of the Creative Commons Attribution licence (https://creativecommons.org/licenses/by/4.0/), which permits unrestricted re-use, distribution, and reproduction in any medium, provided the original work is properly cited.

https://doi.org/10.1017/jfm.2021.808 Published online by Cambridge University Press

twice or three times the significant wave height, which are usually called freak waves. Regev *et al.* (2008) used the one-dimensional Alber equation to study the probability of freak waves initialized by a Gaussian-shaped spectrum.

The Alber equation used by Stiassnie *et al.* (2008) is limited to infinite depths. Here we devote our attention to waves on the continental shelf and the following coastal waters. We use the appropriate cubic Schrödinger equation, and derive from it the relevant Alber equation designed for finite variable depths.

There are three fundamental differences between the model of Alber (1978) and the one presented in this study. In Alber's original equation, in the absence of a disturbance, the linear solution is homogeneous and it is valid for the entire free surface at any time. The inhomogeneous disturbance is introduced over the entire free surface at $t = 0$ and its subsequent nonlinear long-time evolution is valid for $t \geq 0$, it is periodic in x and often also recurrent in t. In our model, in the absence of disturbances the linear solution is stationary, and valid for $x \geq x_0$ and any time t, where x_0 is a reference point. The non-stationary disturbance (periodic in time) is introduced at $x = x_0$ as some type of boundary condition. Last, the nonlinear long-distance evolution is valid for $x \geq x_0$, is assumed periodic in t, and for constant depth is often recurrent in x.

Herein we choose to treat two types of bathymetries: (i) with constant depth $h = 100$ m or $h = 1000$ m; (ii) with constant slope, having a variable depth $h = -0.005x$, for $x \in [x_0, x_e] = [-20\text{ km}, -2\text{ km}]$, with $h \in [100\text{ m}, 10\text{ m}]$ correspondingly, and $x = 0$ at the coastline.

For the attacking stationary wave field, we take a narrow rectangular spectrum, with steepness $\varepsilon = 0.1$, and with carrier frequency $\Omega = 0.77\ \text{s}^{-1}$, which corresponds to a deep-water wavelength of approximately 104 m. Note that for $h = 20$ m, $Kh \approx 1.36$, where K is the carrier wavenumber.

This paper is organized as follows. In § 2 we present the shoaling model, a variable coefficient cubic Schrödinger equation with its corresponding Alber equation. Section 3 deals with the stability of a stationary shoaling wave field. Section 4 describes the numerical method used to compute the long-distance evolution of an unstable wave field, and in § 5 the computations are used to establish the spatio-temporal distribution of wave energy density. The probability of freak-wave occurrence along the shoaling region is calculated in § 6.

2. Background and formulation

The deterministic evolution of a nonlinear, shoaling, ocean wave field (in time t and along the x-axis) with a narrow spectral band is governed by a cubic Schrödinger equation, see (Iusim & Stiassnie 1985):

$$\mathrm{i}\frac{\partial \psi}{\partial X} + \frac{\partial^2 \psi}{\partial T^2} + \mu(X)\,|\psi|^2\,\psi = 0, \tag{2.1}$$

where $\psi(T, X)$ is a dimensionless complex envelope, centred around the carrier wave with constant frequency Ω, related to the free surface elevation by

$$\eta(x,t) = \frac{\varepsilon}{2}\left(\frac{g^3}{2\Omega^5\Omega'}\right)^{1/2}\left[\psi \exp \mathrm{i}\left(\int_{x_0}^{x} K\,\mathrm{d}x - \Omega t\right) + \text{c.c.}\right]. \tag{2.2}$$

In (2.1) the dimensionless parameter μ and dimensionless coordinates are given by

$$\mu = -\frac{g^3\Omega'\alpha_1}{\Omega^7\Omega''}, \quad X = \varepsilon^2\Omega^2\int_{x_0}^{x}\frac{\Omega''\,\mathrm{d}x}{2\,(\Omega')^3}, \quad T = \varepsilon\Omega\left(\int_{x_0}^{x}\frac{\mathrm{d}x}{\Omega'} - t\right). \tag{2.3a–c}$$

https://doi.org/10.1017/jfm.2021.808 Published online by Cambridge University Press

Here K is the carrier local wavenumber given by the linear dispersion relation

$$\Omega^2 = gK \tanh\left(Kh(x)\right), \tag{2.4}$$

with $h(x)$ the variable depth, where $\Omega' = \mathrm{d}\Omega/\mathrm{d}K$ (the carrier group velocity), $\Omega'' = \mathrm{d}^2\Omega/\mathrm{d}K^2$, g is the acceleration due to gravity, ε is the typical wave steepness and

$$\alpha_1 = \frac{gK^3}{2\Omega}\frac{9\tanh^4(Kh) - 10\tanh^2(Kh) + 9}{8\tanh^3(Kh)} - \left(\frac{g^2K}{2\Omega} + \frac{gK\Omega'}{2\sinh(2Kh)}\right)\frac{K}{gh - (\Omega')^2} - \left(\frac{gKh}{2\sinh(2Kh)} + \frac{gK\Omega'}{2\Omega}\right)\frac{gK^2}{2\Omega\left[gh - (\Omega')^2\right]\cosh^2(Kh)}. \tag{2.5}$$

The parameter μ is a variable depth extension of the Zakharov kernel for finite depth $T_{K,K,K,K}$; the latter was obtained by Janssen & Onorato (2007). This kernel governs the modulational instability of narrow-banded wave trains. In shallow depths $\mu < 0$, and in deep water $\mu > 0$, it changes sign for Kh close to 1.363. Note that Iusim & Stiassnie (1985) have derived the current Schrödinger equation (2.1) from their equation (3.1) which has the same left-hand side as equation (1) in the recent paper by Rajan, Bayram & Henderson (2016).

Generally, it is assumed that (2.1) and (2.2) describe the evolution also when the envelope $\psi(T, X)$, and therefore $\eta(x, t)$, are random functions. Using an approach similar to that of Alber (1978), and using a fourth-order moment-closure hypothesis, (2.1) yields the Alber equation for shoaling waves:

$$\mathrm{i}\frac{\partial\rho(T,\tau,X)}{\partial X} + 2\frac{\partial^2\rho(T,\tau,X)}{\partial T\partial\tau} + 2\mu(X)\rho(T,\tau,X)\left[\rho\left(T+\frac{\tau}{2},0,X\right) - \rho\left(T-\frac{\tau}{2},0,X\right)\right] = 0, \tag{2.6}$$

where

$$\rho(T,\tau,X) = \left\langle\psi\left(T+\frac{\tau}{2},X\right)\psi^*\left(T-\frac{\tau}{2},X\right)\right\rangle \tag{2.7}$$

is the two-time correlation function and $\langle\cdot\rangle$ denotes the ensemble average.

In Appendix A, we show that for a linear stochastic shoaling problem, with spectrum $S_0(\omega)$ at x_0, $\rho(T, \tau, X)$ depends only on τ and is given by

$$\rho_s(\tau) = \frac{2\Omega^4}{\varepsilon^2 g^2}\int_0^\infty \exp\mathrm{i}\left[(\omega-\Omega)\tau/(\varepsilon\Omega)\right]S_0(\omega)\,\mathrm{d}\omega, \tag{2.8}$$

which is a trivial solution of Alber equation (2.6).

3. Linear stability analysis

In order to study the instability of stationary shoaling wave fields to non-stationary disturbances, we adapt and follow the approach of Stiassnie *et al.* (2008), whereby a solution is considered in the form

$$\rho(T,\tau,X) = \rho_s(\tau) + \delta R(\tau)\left(\exp\left[\mathrm{i}(\alpha T - \beta X)\right] + \text{c.c.}\right), \tag{3.1}$$

where $\delta = o(1)$ is a dimensionless non-stationarity parameter, α is the frequency of the disturbance and β is its wavenumber. The instability occurs when $\mathrm{Im}(\beta)$ is non-zero.

https://doi.org/10.1017/jfm.2021.808 Published online by Cambridge University Press

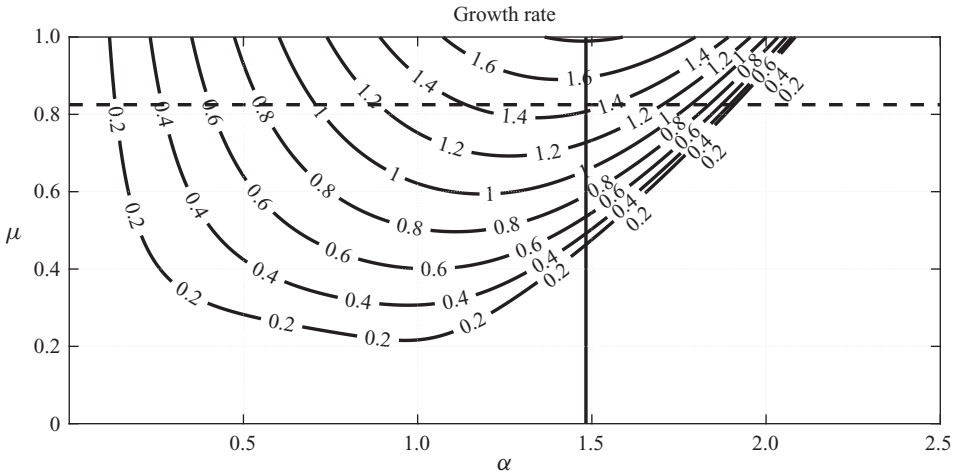

Figure 1. Growth rate as a function of α and μ for fixed $\hat{W} = 1$. The growth rate vanishes for shallow water, i.e. for negative μ. The dashed line shows $\mu = 0.825$, whereas the solid line shows $\alpha = 1.48$ which is a maximum for $\mu = 1$.

Substituting (3.1) into (2.6) and neglecting all terms of order δ^2, leads to a first-order linear ordinary differential equation for $R(\tau)$, which has a straightforward solution decaying when τ tends to infinity. Using (2.8) for ρ_s and evaluating at $\tau = 0$ produces the following dispersion relation for the disturbance:

$$1 = -8\mu\,(X)\,\Omega^6 g^{-2}\alpha^2 \int_0^\infty \frac{S_0(\omega)\,\mathrm{d}\omega}{[2\,(\Omega-\omega)\,\alpha + \varepsilon\Omega\beta]^2 - \varepsilon^2\Omega^2\alpha^4}, \tag{3.2}$$

which is independent of the choice of $R(\tau)$.

For a rectangular spectrum of width $2W$ and height s_0,

$$S_0 = s_0 \quad \text{for } \Omega - W < \omega < \Omega + W, \quad s_0 = \frac{g^2\varepsilon^2}{4W\Omega^4}, \tag{3.3}$$

(3.2) reduces to

$$\frac{\beta^2}{\alpha^2} = \frac{\left(\hat{W}-\alpha\right)^2 - \left(\hat{W}+\alpha\right)^2 \exp\left[-\alpha\hat{W}/\mu\right]}{1-\exp\left[-\alpha\hat{W}/\mu\right]}, \quad \text{where } \hat{W} = \frac{2W}{\varepsilon\Omega}. \tag{3.4}$$

Note that the rectangular spectrum (3.3) and (2.8) give the following stationary solution:

$$\rho_s\,(\tau) = \frac{\sin\left(0.5\hat{W}\tau\right)}{0.5\hat{W}\tau}. \tag{3.5}$$

The growth rate, which is the imaginary part of β, depends on three variables: α, $\hat{W}$ and μ. Figure 1 presents the values of the growth rate for $\hat{W} = 1$, which is the value that we have chosen in our examples.

From figure 1, one can see that the maximum growth rate for infinite depth ($\mu = 1$) is at $\alpha = 1.48$, and the maximum growth rate at 100 m depth (where $\mu = 0.825$) is $\alpha = 1.36$. We have decided to use $\alpha = 1.5$ as input in our calculations.

https://doi.org/10.1017/jfm.2021.808 Published online by Cambridge University Press

Note that in our presentation, we have defined the small parameter ε through the spectrum $S_0(\omega)$ and the carrier wavenumber K_0 (both at x_0), by:

$$\varepsilon = K_0 \left(2 \int_0^\infty S_0(\omega)\, \mathrm{d}\omega \right)^{1/2}. \tag{3.6}$$

4. Numerical approach

In order to study the nonlinear long-distance evolution of a non-stationary shoaling wave field, we adapt the numerical method developed by Stiassnie *et al.* (2008) to our case.

Since the Alber equation is given for three variables (T, τ, X), the numerical domain consists of a finite box $[0, T_{end}] \times [0, \tau_{end}] \times [0, X_{end}]$. Along the T-axis the domain is divided into $N+1$ evenly spaced points, with spacing ΔT. Along the τ-axis the domain consists of $M+1$ evenly spaced points. The ratio $\Delta T/\Delta\tau = 0.4$ is kept fixed. Along the X-axis we took $L+1$ steps. The size of the step ΔX_l is variable. It was chosen as the image, of a uniform grid of $L+1$ steps in the physical domain $[x_0, x_e]$, through the second equation in (2.3*a–c*). In our calculation herein, we use $N = 100$, $M = 1200$, $L = 2\,000\,000$.

Next, we employ a finite difference scheme. The X derivative is approximated by a forward difference and the second partial derivative with respect to T and τ is approximated by a central difference. This gives the following scheme:

$$\begin{aligned}\rho\,(n, m, l+1) = \rho\,(n, m, l) + \frac{\mathrm{i}\Delta X_l}{2\Delta T \Delta\tau} \big(\rho\,(n+1, m+1, l) - \rho\,(n-1, m+1, l) \\ -\rho\,(n+1, m-1, l) + \rho\,(n-1, m-1, l)\big) + 2\mathrm{i}\mu\,(l)\,\Delta X_l \rho\,(n, m, l) \\ \times \left[\rho\left(n + \frac{m\Delta\tau}{2\Delta T}, 0, l\right) - \rho\left(n - \frac{m\Delta\tau}{2\Delta T}, 0, l\right)\right].\end{aligned} \tag{4.1}$$

for $n = 0, \ldots, N$, $m = 0, \ldots, M$, $l = 0, \ldots, L$, where $\rho(n, m, l)$ is a shorthand notation for $\rho(n, m, l) = \rho(n\Delta t, m\Delta\tau, l\Delta X_l)$.

The boundary condition (at $X = 0$) is derived from (3.1) by choosing $R(\tau)$ to be the stationary solution, and thus

$$\rho\,(T, \tau, 0) = \rho_s\,(\tau)\,(1 + 2\delta \cos(\alpha T))\,. \tag{4.2}$$

In our examples, we took $\delta = 0.05$, $\alpha = 1.5$, and for $\rho_s(\tau)$ we take the expression (3.5) derived for the rectangular spectrum (3.3) with $W = 0.5\varepsilon\Omega$ and $s_0 = g^2\varepsilon/2\Omega^5$.

A periodicity condition is used along the T-axis with period $2\pi/\alpha$, where α is the frequency of the initial disturbance. We also use the symmetry condition arising from the definition (2.7) of the two-time correlation function: $\rho(n, -m, t) = \rho^*(n, m, t)$. Last, a condition for large τ is introduced, for which we use an equation similar to (A7) in Ribal *et al.* (2013).

To check the quality of our numerical results, we used the fact that (2.6) has three invariants, as outlined in Appendix B.

5. Long-distance evolution

The variance of the free-surface elevation, associated with a random wave field, can be written as

$$\langle \eta^2(x, t)\rangle = \frac{\varepsilon^2 g^3}{4\Omega^5\Omega'}\rho(T, 0, X). \tag{5.1}$$

https://doi.org/10.1017/jfm.2021.808 Published online by Cambridge University Press

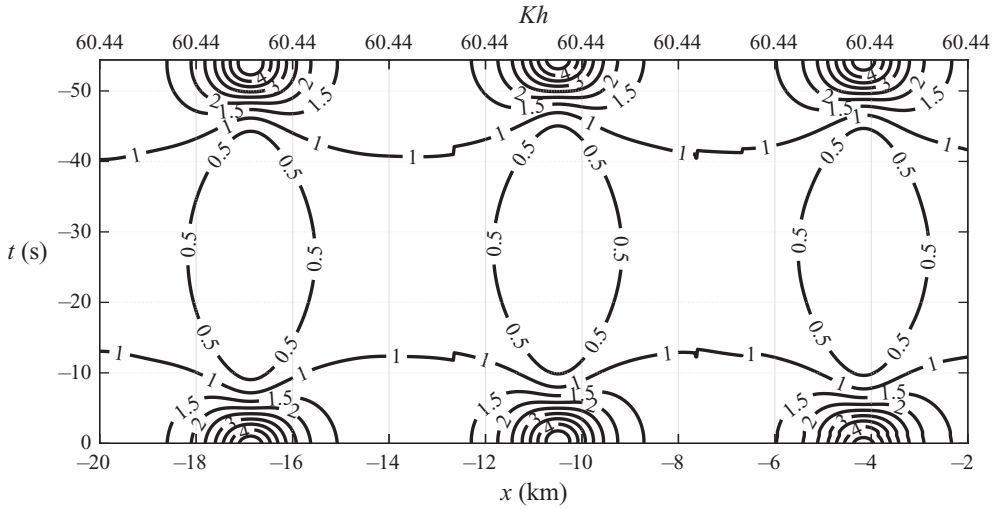

Figure 2. Long-distance evolution of the normalized variance $\tilde{\rho}$, for constant depth, $h = 1000$ m. The upper x-axis shows the value of Kh.

Its significance comes from the fact that it is proportional to the energy density of the wave field, see Holthuijsen (2010). Thus the importance of the Alber equation is related to the fact that it models the long-distance evolution of wave energy.

In the linear case, by means of (A4), the variance of the linear solution of the free surface, at $x = x_0$, reduces to

$$\langle \eta_L^2(x_0) \rangle = \frac{\varepsilon^2 g^2}{2\Omega^4} \rho_s(0), \tag{5.2}$$

which is used to normalize the variance (5.1):

$$\tilde{\rho} = \frac{\langle \eta^2 \rangle}{\langle \eta_L^2(x_0) \rangle} = \frac{g}{2\Omega\Omega'} \frac{\rho}{\rho_s(0)}. \tag{5.3}$$

In order to get a clear picture of the evolution of $\tilde{\rho}$ across the space–time domain, and owing to the spacial periodicity with respect to t, the results were shifted periodically so that its maximum always appears at $t = 0$. The long-distance evolution of $\tilde{\rho}$, for the different examples, is shown in figures 2–4.

From figures 2 and 3, one can see that for constant depths the evolution is recurrent. The solution exhibits the typical behaviour of a homogeneous wave field in infinite depth with an initial inhomogeneous disturbance as input. The evolution of $\tilde{\rho}$ can be described as a sequence of consecutive recurrent cells. In each cell, the variance begins close to rest (all values close to 1) and then there is a concentration of wave energy, and $\tilde{\rho}$ attains its maximum value. Then the process is reverted and the variance falls back to a somewhat relaxed state around the rest position $\tilde{\rho} \equiv 1$.

Depth influences the particular details of the evolution; for 1000 m depth the cell length is 6.4 km and reaches a maximum value of 4.8, meaning that at such a specific point the wave energy is almost fivefold that of the input wave field. At $x \approx -17$ (where the maximum occurs) for most of the values of t, $\tilde{\rho} < 0.5$, showing that the wave energy is being concentrated in the vicinity of a single point. Note that the total energy is conserved, as given by the first invariant in Appendix B. For 100 m depth, the cell length increases to 7.6 km and the maximum of $\tilde{\rho}$ decreases to 4.2.

https://doi.org/10.1017/jfm.2021.808 Published online by Cambridge University Press

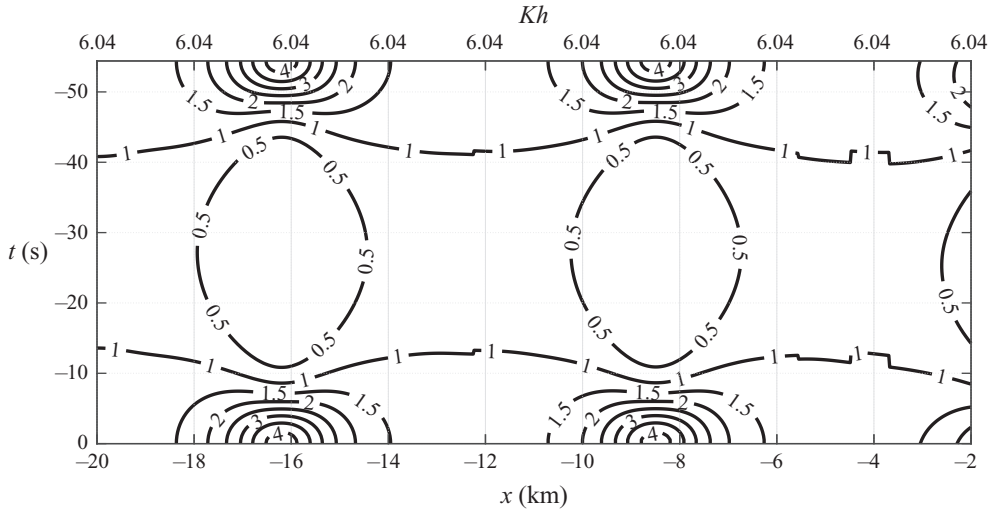

Figure 3. Long-distance evolution of the normalized variance $\tilde{\rho}$, for constant depth, $h = 100$ m. The upper x-axis shows the value of Kh.

For the shoaling case, the behaviour is dramatically different. From figure 4, one can see that the cellular structure is persistent but the cells are different from each other. The variance goes through a sequence of four cells, each of which shows focusing of wave energy albeit decaying as the depth decreases. Over the first 6 km (cell I), the effect of variable depth is negligible and $\tilde{\rho}$ behaves as in constant depth; it shows a similar pattern and reaches almost the same maximum value as shown in figure 3. Over the next 5 km (cell II), one can see a second and somewhat shorter cell where the maximum of $\tilde{\rho}$ decreases to 2.8. Along the next 4 km (cell III), there is less energy concentration with a maximum of $\tilde{\rho}$ decreasing to 1.8; the energy concentration is reduced almost by half compared with the initial cell. Over the last 2 km of the domain (cell IV), there is no meaningful concentration of energy; the phenomena has disappeared and the sea state is effectively similar to a stationary wave field. Over the last cell $\mu < 0$ and, similar to the deterministic case, the instability vanishes.

In order to assess the quality of our numerical simulations, we check the conservation of the invariants, which are given in Appendix B. The first invariant is the most meaningful because it is related to the total energy. In all the examples, $I_1 = 4.18$ and it was successfully preserved by the numerical solver, with relative errors of the order of $O(10^{-7})$. The second invariant is always zero. The third invariant, which is only valid for constant depth, was $I_3 = 3.79$ for $h = 1000$ m and $I_3 = 3.12$ for $h = 100$ m. This invariant depends both on the values along $\tau = 0$ and the values along the τ-axis. The relative deviation from its value at $X = 0$ did not exceed half a percentage throughout the nonlinear computation.

6. Probability of freak-wave occurrence

The probability distribution of the wave height of a Gaussian narrow-banded wave field, is given by the Rayleigh distribution, see Holthuijsen (2010). Thus, at any given (t, x) the

https://doi.org/10.1017/jfm.2021.808 Published online by Cambridge University Press

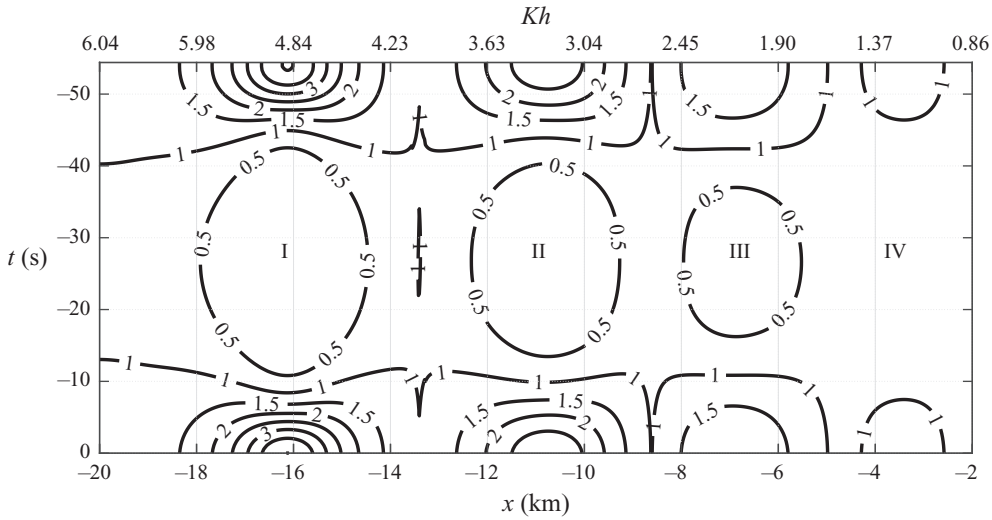

Figure 4. Long-distance evolution of the normalized variance $\tilde{\rho}$, for shoaling waters. The upper x-axis shows the local values of Kh.

probability to obtain waveheights H larger than $\hat{H}$ is:

$$F(\hat{H}, t, x) = P(H > \hat{H}) = \exp\left[-\left(\frac{\hat{H}}{H_{rms}(t, x)}\right)^2\right], \tag{6.1}$$

where H_{rms} denotes the root-mean-square wave height and it is related to the variance of the free-surface elevation by $H_{rms} = \sqrt{8\langle\eta^2(x, t)\rangle}$, where $\langle\eta^2(x, t)\rangle$ is given by (5.1).

It is useful to compare H_{rms} with the root-mean-square wave height of the linear solution taken at a reference point x_R, so we define $H_{rms0} = \sqrt{8\langle\eta_L^2(x_R)\rangle}$, where $\langle\eta_L^2(x_R)\rangle$ is given below in (6.4), and upon normalizing H_{rms}, the probability of wave height exceedance at (x, t) becomes

$$F(\hat{H}, t, x) = P(H > \hat{H}) = \exp\left[-\left(\frac{\hat{H}}{H_{rms0}}\right)^2 \frac{\langle\eta_L^2(x_R)\rangle}{\langle\eta^2(x, t)\rangle}\right]. \tag{6.2}$$

The relevant probability over a certain domain is found by averaging over such domain. Since the evolution of $\tilde{\rho}$ naturally defines different regions of interest, i.e. the recurrent cells shown in figures 2, 3 and the variable cells in figure 4, the probability of wave exceedance over each cell is given by

$$P(H \geq \hat{H}) = \frac{1}{(x_2 - x_1)t_{max}} \int_0^{t_{max}} \int_{x_1}^{x_2} F(\hat{H}, t, x)\, \mathrm{d}x\, \mathrm{d}t. \tag{6.3}$$

Here $t_{max} = 54$s is the period of $\tilde{\rho}$ with respect to t, x_1 is the beginning of the cell under consideration and x_2 is its endpoint. In the constant depth cases, the reference point $x_R = x_1 = x_0$. For the shoaling case, $x_R = (x_1 + x_2)/2$, the middle point of each of the cells.

Equation (6.3) was derived by Andrade & Stiassnie (2020) and was shown to be equivalent to the original equation derived by Regev *et al.* (2008).

https://doi.org/10.1017/jfm.2021.808 Published online by Cambridge University Press

Case	cell	H_s	$P(H \geq 2H_s)$	P/R	$P(H \geq 3H_s)$	P/R
$h = 1000$ m	any	4.67 m	6.60×10^{-3}	19.67	0.35×10^{-3}	2.32×10^4
$h = 100$ m	any	4.67 m	5.99×10^{-3}	17.86	0.23×10^{-3}	1.56×10^4
Shoaling	I	4.67 m	7.01×10^{-3}	20.91	0.25×10^{-3}	1.66×10^4
	II	4.65 m	4.64×10^{-3}	13.85	0.06×10^{-3}	4.46×10^3
	III	4.49 m	2.53×10^{-3}	7.56	0.01×10^{-3}	731.9
	IV	4.27 m	0.58×10^{-3}	1.73	0.13×10^{-6}	8.55

Table 1. Probability of freak-wave occurrence. The values taken from the Rayleigh distribution are 0.33×10^{-3} for wave heights higher than $2H_s$, 0.15×10^{-7} for wave heights higher than $3H_s$. The columns P/R are the ratios between the calculated probabilities and their corresponding values from the Rayleigh distribution.

Following Holthuijsen (2010) the significant wave height is well approximated by $H_s = 4\sqrt{\langle \eta_L^2 \rangle}$. The variance of the linear free surface at x_R is

$$\langle \eta_L^2(x_R) \rangle = \frac{\varepsilon^2 g^3}{4\Omega^5 \Omega'(x_R)}. \tag{6.4}$$

The main result of this section, the probabilities of freak-wave occurrence, is given in table 1.

In the cases of constant depth, due to the recurrence, only the values obtained during the first cell are shown in table 1 because they hardly differ from one cell to another. In 1000 m depth the probability of freak-wave occurrence is increased 20 times and in 100 m depth it is increased by a factor of 17 with respect to the Rayleigh distribution. By looking at extreme wave heights, higher than three times H_s, the probability is increased by 20 000 fold, making freak-waves encounter a feasible event.

In the case of shoaling, the results show that the probability of freak waves decreases with depth. In the deeper region, the probabilities are similar to those obtained for constant 100 m depth. From there on they decrease rapidly and towards the end of domain, in the shallower region, the probabilities are closer to the Rayleigh distribution.

Funding. The authors are grateful for the support of the Israeli Science Foundation, grant 261/17.

Declaration of interests. The authors report no conflict of interest.

Author ORCIDs.
Mateusz Kluczek https://orcid.org/0000-0002-7954-4478;
David Andrade https://orcid.org/0000-0002-9486-8200.

Appendix A

Following (Pierson 1955), a stationary Gaussian unidirectional wave field is given by the integral

$$\eta_L(x, t) = \frac{1}{2} \int_0^\infty \exp \mathrm{i} \left[\int_{x_0}^x k(\omega)\, \mathrm{d}x - \omega t + \theta(\omega) \right] \sqrt{2S(x, \omega)\, \mathrm{d}\omega} + \text{c.c.}, \tag{A1}$$

where $k(\omega)$ is given by the linear dispersion relation, $\theta(\omega)$ is a random phase with uniform distribution in $(-\pi, \pi]$, and $S(x, \omega)$ is the energy spectrum at the point x.

https://doi.org/10.1017/jfm.2021.808 Published online by Cambridge University Press

According to the linear theory of shoaling waves, for each x the following relation holds:

$$c_g(x_0, \omega)S_0(\omega) = c_g(x, \omega)S(x, \omega), \tag{A2}$$

where c_g denotes the local group velocity and $S_0(\omega)$ is the wave spectrum at the reference point x_0. The general form of a stationary Gaussian, shoaling wave field is

$$\eta_L(x, t) = \frac{1}{2}\int_0^\infty \exp \mathrm{i}\left[\int_{x_0}^x k(\omega)\,\mathrm{d}x - \omega t + \theta(\omega)\right]\sqrt{2S_0(\omega)\frac{c_g(x_0, \omega)}{c_g(x, \omega)}\,\mathrm{d}\omega} + \text{c.c.} \tag{A3}$$

Assuming that the spectrum is narrow banded, the following approximation, valid to order ε, is made: $c_g(x_0, \omega)/c_g(x, \omega) = \Omega'(x_0)/\Omega'$. This is substituted into (A3) to get

$$\eta_L(x, t) = \frac{1}{2}\left(\frac{2\Omega'(x_0)}{\Omega'}\right)^{1/2}\int_0^\infty \exp \mathrm{i}\left[\int_{x_0}^x k(\omega)\,\mathrm{d}x - \omega t + \theta(\omega)\right]\sqrt{S_0(\omega)\,\mathrm{d}\omega} + \text{c.c.} \tag{A4}$$

Comparing (A4) with (2.2) yields the complex envelope which is given by

$$\psi(x, t) = \frac{2}{\varepsilon}\left(\frac{\Omega^5\Omega'(x_0)}{g^3}\right)^{1/2}\int_0^\infty \exp \mathrm{i}\left[\int_{x_0}^x (k - K)\,\mathrm{d}x - (\omega - \Omega)t + \theta(\omega)\right]\sqrt{S_0(\omega)\,\mathrm{d}\omega}, \tag{A5}$$

Note that ψ is a Gaussian stationary random process. Therefore, the two-time correlation depends only on the time difference and so, for any x, t_1 and t_2,

$$\langle\psi(x, t_1)\psi^*(x, t_2)\rangle = \frac{4\Omega^5\Omega'(x_0)}{\varepsilon^2 g^3}\int_0^\infty \exp \mathrm{i}\left[(\omega - \Omega)(t_1 - t_2)\right]S_0(\omega)\,\mathrm{d}\omega. \tag{A6}$$

Switching from the physical variables x and t to X and T, denoting by $\tau = \varepsilon\Omega(t_1 - t_2)$ the dimensionless time separation, one obtains the correlation function of a stationary (independent of T and X) shoaling wave field:

$$\rho_S(\tau) = \rho(T, \tau, X) = \frac{4\Omega^5\Omega'(0)}{\varepsilon^2 g^3}\int_0^\infty \exp \mathrm{i}\left[(\omega - \Omega)\tau/(\varepsilon\Omega)\right]S_0(\omega)\,\mathrm{d}\omega. \tag{A7}$$

Note that x_0, the initial point of the physical domain, corresponds to $X = 0$ in the dimensionless coordinates.

Last, assuming that at $X = 0$ the water depth is sufficiently deep so that $\Omega'(0) = g/(2\Omega)$ in (A7), yields (2.8).

Appendix B

The Alber equation (2.6) has three invariants. Following a similar approach to that of (Ribal *et al.* 2013), the first and second invariants are

$$I_1 = \int \rho(T, \tau, X)|_{\tau=0}\,\mathrm{d}T; \quad I_2 = \int \frac{\partial}{\partial\tau}\rho(T, \tau, X)\bigg|_{\tau=0}\mathrm{d}T = 0. \tag{B1a,b}$$

The third invariant is

$$I_3 = \mu(X)\int \rho^2(T, \tau, X)\bigg|_{\tau=0}\mathrm{d}T + \int \frac{\partial^2}{\partial\tau^2}\rho(T, \tau, X)\bigg|_{\tau=0}\mathrm{d}T. \tag{B2}$$

Note that I_3 is only valid for constant depths.

https://doi.org/10.1017/jfm.2021.808 Published online by Cambridge University Press

References

Alber, I.E. 1978 The effects of randomness on the stability of two-dimensional surface wavetrains. *Proc. R. Soc. Lond.* A **363**, 525–546.

Andrade, D. & Stiassnie, M. 2020 New solutions of the C.S.Y. equation reveal increases in freak wave occurrence. *Wave Motion* **97**, 102581.

Holthuijsen, L.H. 2010 *Waves in Oceanic and Coastal Water*. Cambridge University Press.

Iusim, R. & Stiassnie, M. 1985 Shoaling of nonlinear wave-groups on water of slowly varying depth. *Z. Angew. Math. Phys.* **36**, 680–690.

Janssen, P. & Onorato, M. 2007 The intermediate water depth limit of the Zakharov equation and consequences for wave prediction. *J. Phys. Oceanogr.* **37** (10), 2389–2400.

Longuet-Higgins, M.S. 1976 On the nonlinear transfer of energy in the peak of a gravity-wave spectrum: a simplified model. *Proc. R. Soc. Lond.* A **347** (1650), 311–328.

Pierson, W. 1955 Wind generated gravity waves. In *Advances in Geophysics*, vol. 2, pp. 93–178. Elsevier.

Rajan, G.K., Bayram, S. & Henderson, D.M. 2016 Periodic envelopes of waves over non-uniform depth. *Phys. Fluids* **28** (4), 042106.

Regev, A., Agnon, Y., Stiassnie, M. & Gramstad, O. 2008 Sea-swell interaction as a mechanism for the generation of freak waves. *Phys. Fluids* **20** (11), 112102.

Ribal, A., Babanin, A.V., Young, I., Toffoli, A. & Stiassnie, M. 2013 Recurrent solutions of the Alber equation initialized by Joint North Sea Wave Project spectra. *J. Fluid Mech.* **719**, 314–344.

Stiassnie, M., Regev, A. & Agnon, Y. 2008 Recurrent solutions of Alber's equation for random water-wave fields. *J. Fluid Mech.* **598**, 245–266.

https://doi.org/10.1017/jfm.2021.808 Published online by Cambridge University Press